THE ASTROPHYSICAL JOURNAL, 448:356–364, 1995 July 20

COMPTON GAMMA-RAY OBSERVATORY OBSERVATIONS OF THE CRAB PULSAR

M. P. ULMER, S. M. MATZ, AND D. A. GRABELSKY
Department of Physics and Astronomy, Northwestern University, Evanston, IL 60208-3112
J. E. GROVE AND M. S. STRICKMAN
Code 7650, E. O. Hulburt Center for Space Research, Naval Research Laboratory, Washington, DC 20375
R. MUCH AND M. C. BUSETTA
Astrophysics Division, ESTEC, NL-2200 AG Noordwijk, The Netherlands
A. STRONG
Max-Planck Institut für extraterrestrische Physik, Giessenbachstrasse, Postfach 1603, 85740 Garching, Germany
L. KUIPER
SRON-Utrecht, Sorbonnelaan 2, 3584 CA Utrecht, The Netherlands
D. J. THOMPSON AND D. BERTSCH
Code 662, NASA Goddard Space Flight Center, Greenbelt, MD 20771
AND
J. M. FIERRO AND P. L. NOLAN
W. W. Hansen Experimental Physics Laboratory and Department of Physics, Stanford University, Stanford, CA 94305
Received 1994 November 9; accepted 1995 January 31

ABSTRACT

We present Crab pulsar light curves and spectra over the ~50 keV to 10 GeV range from *Compton Gamma-Ray Observatory* observations made during MJD 48,373–48,406 (1991 April 27–1991 May 30, except for COMPTEL which started observations on April 28). The overall pulse phase–averaged spectrum is not well fitted by a single power law, but a broken power law does fit well, of the form $F = A(E/E_B)^{(-\alpha_1)}$; $A(E/E_B)^{(-\alpha_2)}$ photons cm^{-2} s^{-1} MeV^{-1} fits well ($\chi^2_{\rm min} = 16$, 26 degrees of freedom [dof]), where α_1 is the spectral index for $E \leq E_B$ and α_2 for $E > E_B$. For the normalization values to the spectra quoted here, we report phase-averaged intensities, and we applied an estimate to the uncertainty of the absolute calibration of 10%.

The best-fit values for the parameters with 68% uncertainties are $A = 0.064 \pm 0.006$, $E_B = 0.12 \pm 0.03$ MeV, $\alpha_1 = 1.71^{+0.15}_{-0.19}$, and $\alpha_2 = 2.21 \pm 0.02$. The outer gap model (with gap parameter equal to 0.38, and a normalization factor of 1.08) provided to us by Ho describes the data with an accuracy of better than 20%, but the formal $\chi^2_{\rm min}$ is too high with a value of 68 for 28 dof. We derive a statistically equivalent result for the broken power law when we include lower energy data from the *OSO 8* satellite.

A broken power-law fit to the phase-resolved spectra (peak 1, the bridge, and peak 2) resulted in the following: for peak 1, $A = 0.026 \pm 0.003$, $E_B = 0.098 \pm 0.02$ MeV, $\alpha_1 = 1.77^{+0.18}_{-0.25}$, $\alpha_2 = 2.09 \pm 0.01$, $\chi^2_{\rm min} = 45$, 26 dof; for the bridge, $A = 0.001 \pm 0.0001$, $E_B = 0.45^{+0.85}_{-0.15}$ MeV, $\alpha_1 = 1.75 \pm 0.12$, $\alpha_2 = 2.53^{+0.10}_{-0.12}$, $\chi^2_{\rm min} = 16$, 23 dof; and for peak 2, $A = 0.02 \pm 0.002$, $E_B = 0.13^{+0.020}_{-0.012}$ MeV, $\alpha_1 = 1.71 \pm 0.09$, $\alpha_2 = 2.25 \pm 0.02$, $\chi^2_{\rm min} = 21$, 26 dof. For peak 1 only, the fit is greatly improved by using an outer gap model. The resultant values are a gap parameter of 0.450 ± 0.003 with a normalization of 0.22 ± 0.02, $\chi^2_{\rm min} = 32$, 28 dof.

The separation of the pulse peaks is difficult to quantify objectively because the peaks are not symmetrical. When we use the maximum intensity values of each peak to determine the centroids, we find an energy-independent phase difference of 0.405 ± 0.006 for the *CGRO* data (50 keV to 10 GeV) and 0.402 ± 0.002 when other data were included covering the range from 0.5 to 300 keV. The energy-independent value of the phase of peak 1 relative to the radio is -0.003 ± 0.012, where the uncertainty includes the absolute timing uncertainty.

When the pulse shapes are characterized by asymmetric Lorentzian shapes, within the statistical uncertainty of the fits, the widths of the peaks in the ~100 keV light curve are consistent within a factor of about 1.25 with the widths of the peaks in the ~100 MeV light curve.

We discuss these results within the context of a bulk relativistic motion beaming model.

Subject headings: gamma rays: observations — pulsars: individual (Crab pulsar)

1. INTRODUCTION

The Crab pulsar has been extensively studied in the hard X-ray to gamma-ray range, but until the launch of the *Compton Gamma-Ray Observatory* (*CGRO*) simultaneous observations in the ~50 keV to 10 GeV energy range were not possible. Since there is some evidence that the light curve is variable over some or all of this energy range (cf. Nolan et al. 1993; Ulmer et al. 1994, and references therein), it is useful to combine the *CGRO* results as opposed to simply combining data from the literature. In addition, the *CGRO* instrument sensitivities are better than those of previous experiments. Furthermore, since our team had access to the raw data, we were able to analyze all the data in a consistent manner, accumulating the spectra over the same range of phase bins for the entire

50 keV to 10 GeV energy range using the same pulsar ephemeris and satellite clock system. Here we report the results of the analysis of the three pointed instruments on the *CGRO*: the Oriented Scintillation Spectrometer Experiment (OSSE), the Compton Telescope (COMPTEL), and the Energetic Gamma Ray Experiment Telescope (EGRET).

Previous models of the emission, such as those of Daugherty & Harding (1982), Arons (1984), Cheng, Ho, & Ruderman (1986a, b), Ho (1993), Dermer & Sturner (1994), and Sturner & Dermer (1994), have all concentrated on the average pulse spectrum. Our results suggest, however, that spectral models for different portions of the light curve are important. Based on these results, we suggest an empirical model of the emission regions to explain both the features of the spectra and the light curves.

2. OBSERVATIONS

The observations were made from MJD 48,373 to 48,406 (1991 April 27–1991 May 30; except COMPTEL which began observing on April 28). Detailed descriptions of the observations can be found in Nolan et al. (1993), Ulmer et al. (1994), and Much et al. (1994). Descriptions of the instruments can be found in the following references: OSSE (50 keV to 10 MeV, Johnson et al. 1993), COMPTEL (0.75 MeV to 30 MeV, Schönfelder et al. 1993), and EGRET (20 MeV to 10 GeV, Thompson et al. 1993).

The operation of the spacecraft clock and the time-tagging of the instruments' data are described in detail in the above references. The relative timing among the instruments is good to 0.125 ms, and the absolute timing relative to the radio is good to 0.3 ms (Ulmer et al. 1994; Nolan et al. 1993, and references therein).

3. ANALYSIS AND RESULTS

3.1. *Timing*

Standard pulsar analysis has been described in Ulmer et al. (1993). Briefly, we epoch-folded the data using the relative phases of the detected photons according to the following formula, which converts the arrival time at the solar system barycenter to a phase:

$$\phi(t) = \phi(t_0) + \nu_0(t - t_0) + \dot{\nu}_0(t - t_0)^2/2 + \ddot{\nu}_0(t - t_0)^3/6 \,. \quad (1)$$

The pulsar parameters used in our timing analysis were derived from the radio ephemeris provided by Arzoumanian, Nice, & Taylor (1992; see also Ulmer et al. 1994). For completeness we reproduce the information in Table 1.

TABLE 1

CRAB PULSAR EPHEMERIS

	TJD SPAN	
PARAMETER	8371–8412	8794–8816
ν (s^{-1})	29.9492515379593	29.9350985720614
$\dot{\nu}$ (s^{-2})	-3.77657×10^{-10}	-3.77229×10^{-10}
$\ddot{\nu}$ (s^{-3})	8.18×10^{-21}	1.17×10^{-20}
$T_{0_{geo}}$	8371.000000104 (TJD)	8805.000000153 (TJD)
R.A.(J2000)	$5^h34^m31^s.973$	...
Decl.(J2000)	22°00′52″.06	...
DM (ms)	56.776[a] (5)	56.790 (5)

[a] S. Lundgren & J. Cordes 1991, private communication.

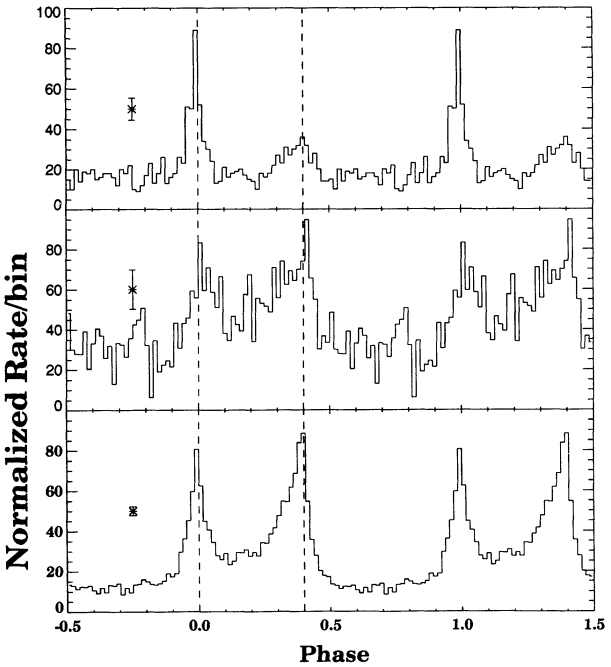

FIG. 1.—Light curve of the Crab pulsar in 64 phase bins plotted for two cycles, for all three *CGRO* instruments. *Top to bottom*: EGRET (greater than 30 MeV), COMPTEL (1–10 MeV), and OSSE (90–130 keV). The dashed vertical lines denote phase 0 and phase 0.4, the typically quoted peak separation. Typical error bars are shown.

3.2. *Light Curve*

3.2.1. *Profile Fits*

For uniformity among the various experiments, we binned the data into 64 equally spaced phase bins (~0.5 ms wide). The light curves (shown in Fig. 1) are characterized by two peaks, referred to as P1 and P2, plus a region between the peaks, referred to as the bridge. The phase definitions (with phase 0.0 as defined by the radio ephemeris) of these regions are reproduced here from Ulmer et al. (1994) in Table 2.

We fitted the light curves in Figure 1 over the peak and bridge regions with a modified asymmetric Lorentzian profile, following Hasinger (1984) and Hasinger et al. (1984).

The functional form that we used to describe the left-hand side of each peak plus background is

$$f(x) = \alpha \Big/ \left[1 + \left(\frac{\beta - x}{\gamma}\right)^{\delta}\right] + \epsilon \,, \quad (2)$$

where β defines the phase of the peak, γ and α are the peak half-widths and amplitudes, x is the phase at which the function is evaluated, δ determines the slope, and ϵ is the background term. For the right-hand side ($x > \beta$) of each peak, the

TABLE 2

DEFINITION OF PHASE INTERVALS OF THE CRAB PULSAR

Region	Phase
Peak 1	0.95–0.05
Bridge	0.08–0.27
Peak 2	0.30–0.44
Background	0.60–0.80
Total composite pulse	0.85–0.55

term with β and γ changes to $(x - \beta)/\gamma$. Unlike Hasinger et al. (1984), we allowed δ to be different for each peak, which led to a description of the peaks and bridge region with an accuracy of typically better than 20%, though the $\chi^2_{\rm min}$ values were not low enough to derive uncertainties for the parameters. It should also be noted that in these fits we allowed the background term to take on a separate value for each peak. In order to provide a single description of the light curves over the entire bridge plus peak, it is necessary to average the two background values; e.g., the net light curve description for the peaks and the bridge is $f_1 - \epsilon_1/2 + f_2 - \epsilon_2/2$, where the subscripts denote the two peaks. For completeness the results of the fits are given in Table 3. As the overall fits to the entire light curve are not statistically rigorous, uncertainties to the parameters are not given.

Besides providing an analytic fit to the data, we also used these fits to characterize the sharpness of the peaks. To quantify what was done by Ulmer (1994), we used the EGRET and OSSE data near the peaks (a total of 11 phase bins around each peak). The value of γ is different for the left and right sides of the peaks. However, to obtain a good fit ($\chi^2_{\rm min} = 11$, 5 dof) to the low-energy data (see Table 3 where we see that the OSSE data have unacceptably large $\chi^2_{\rm min}$ values), it was necessary to use the $\frac{1}{8}$ ms time-tagged OSSE data divided into 256 phase bins (Ulmer et al. 1994). This apparently is simply a matter of binning (e.g., the light curve in Fig. 1 is from the same data, but when the data are binned into 256 phase divisions rather than 64, a better fit is achieved). We then measured the $\chi^2_{\rm min} + 1$ for variations in the value of $\gamma_{\rm left}$ and $\gamma_{\rm right}$, separately, and combined these uncertainties in quadrature to produce the following effective widths (EFWs) in units of phase for P1 and P2: for EGRET, EFW for P1 $= 0.065 \pm 0.007$ and EFW for P2 $= 0.17 \pm 0.4$; and for OSSE, EFW for P1 $= 0.093 \pm 0.04$ and EFW for P2 $= 0.12 \pm 0.04$. We see that the effective widths are comparable for both peaks at the widely disparate OSSE and EGRET energy ranges.

In the above model, a precise determination of the peak phase bin is not possible as the freedom to change the slope of each side of the peak allows for a large ($\gtrsim 0.1$) variance in the value for the peak phase. A Gaussian-shaped fit to the central five or nine phase bins yielded a value of 0.395 ± 0.005 for the peak separation for the *CGRO* data. However, the *Einstein* (0.5–3.5 keV) light curve is too sharp to allow us to include these data in a self-consistent manner with a Gaussian model. Therefore, we determined the peak separation simply from the maximum intensity points for the peaks in the light curve. This approach is insensitive to changes in pulse shape with respect to energy, though it is more sensitive to statistical fluctuations in the phase bins near the peaks. The phase uncertainty we assigned to the data in this case is $\frac{1}{2}$ phase bin (for each peak) and therefore $2^{1/2} \times \frac{1}{2}$ phase bin for the net error in the peak separation. For consistency among the *CGRO* data sets, we confined ourselves to the light curves in Figure 1. We then fitted the resulting phase separations as a function of energy using the *CGRO* data alone. We also considered the *CGRO* data along with the *Einstein* data (Harnden & Seward 1984). The results are that both data sets shown in Figure 2 are consistent with a constant (with respect to energy) peak separation of 0.405 ± 0.005 ($\chi^2_{\rm min} = 0.02$ for the *CGRO* data alone and 0.402 ± 0.002, $\chi^2_{\rm min} = 0.18$ for *CGRO* plus *Einstein*). For completeness (see, for comparison, Ramanamurthy 1994; Thorsett 1991), we also fitted a power law of the form $\delta\theta = A(E/1\ {\rm MeV})^{\alpha}$, where $\delta\theta$ corresponds to the phase separation. The best-fit corresponding values of A and α are $A = 0.403 \pm 0.003$, $\alpha = (0.6 \pm 1.0) \times 10^{-3}$, $\chi^2_{\rm min} = 0.06$.

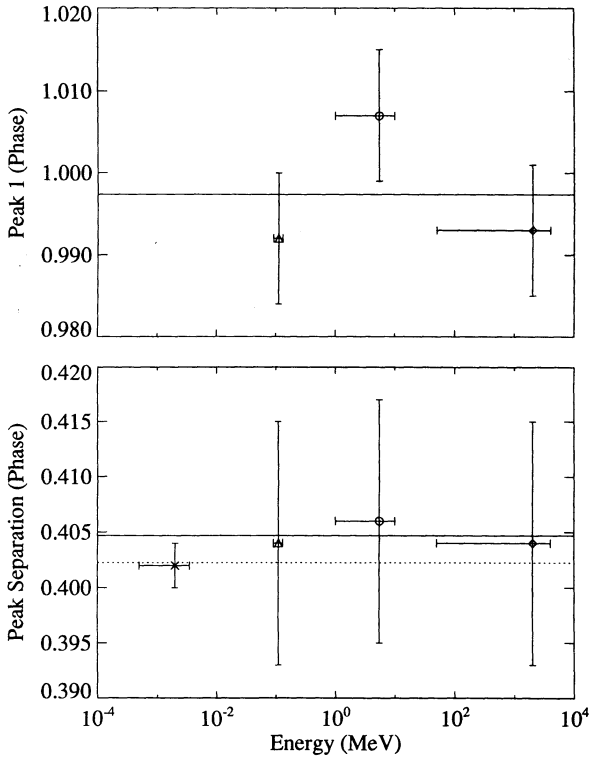

FIG. 2.—Crab pulsar peak phases. The phase of P1 relative to radio (*top*) for (*left to right*) OSSE, COMPTEL, and EGRET, and the phase separation (*bottom*) (*left to right*) of P1 and P2 for *Einstein* (Harnden & Seward 1984), OSSE, COMPTEL, and EGRET. The horizontal lines are the weighted averages; the solid lines include only *CGRO* data.

TABLE 3

SUMMARY OF MODIFIED LORENTZIAN FITS[a]

Instrument (peak)	α	β	γ_l	γ_r	δ	ϵ	$\chi^2_{\rm min}$[b]
OSSE(1).....	63	-1.4×10^{-2}	2.5×10^{-2}	4.4×10^{-2}	1.5	11	23
OSSE(2).....	86	0.40	9.6×10^{-2}	1.8×10^{-2}	1.1	3	9
COMPTEL(1).....	53	2.8×10^{-3}	1.95×10^{-2}	5.5×10^{-2}	0.98	31	10
COMPTEL(2).....	100	0.43	0.12	5.3×10^{-3}	0.57	12	5
EGRET(1).....	65	-1.1×10^{-2}	3.8×10^{-2}	3.7×10^{-2}	1.7	1.3	13
EGRET(2).....	26	0.39	8.9×10^{-2}	7.8×10^{-2}	3.1	4.7	3

[a] $f(x) = \alpha/\{1 + [(\beta - x)/\gamma]^{\delta}\} + \epsilon$; the values of α and ϵ have been scaled to the light curves shown in Fig. 1.

[b] Degrees of freedom equal 5 in all cases.

We performed a similar analysis on the values of the phase of P1 in the *CGRO* data alone (see Fig. 2) and found again that the data were most consistent with no energy dependence (phase relative to the radio of -0.003 ± 0.006, statistical uncertainty only). The net uncertainty is dominated by an uncertainty of 300 μs (3 σ) in the radio absolute timing tabulated in the Princeton *CGRO* data base. This corresponds to a 0.009 phase uncertainty.

3.3. *Spectral Analysis*

In order to perform phase-resolved spectral analysis of the data, we used the phase definitions of P1, P2, the bridge, and background regions as given in Table 2 (see also Ulmer et al. 1994, and references therein). "Background" included unpulsed emission from the pulsar (if any) and emission from the Crab Nebula, as well as detector background.

We converted from counts s^{-1} MeV^{-1} to photons cm^{-2} s^{-1} MeV^{-1} by the following process. Each instrument's data sets were fitted individually using the standard method of forward-folding candidate spectra through the instrument response to produce a best fit to the data. Then these data were converted to photons cm^{-2} s^{-1} MeV^{-1} by multiplying the observed counts s^{-1} MeV^{-1} by the derived ratio of the photons to counts for the best-fit model. We found that the range of conversion values for the spread in uncertainties in the best-fit spectrum was negligible compared to the uncertainties due to counting statistics and the absolute calibration of the instruments.

In Figure 3 we show the composite *CGRO* average Crab pulsar spectrum from 50 keV to 10 GeV. According to convention, we have phase-averaged the flux over the entire light curve; i.e., the instantaneous flux value (derived from the total counts divided by total live time over a specific phase range [Δ]) was multiplied by Δ. We have chosen to phase-average the peak and bridge spectra as well. See Table 2 for phase range definitions that allow conversion back to an "instantaneous" flux.

We fitted all the spectra (total, P1, bridge, and P2) with the following forms: a power-law, a broken power-law, and an outer gap model (Ho 1993). When a good fit was achieved for either a single power-law or outer gap model, we established the uncertainties by assuming the spectral index (or outer gap parameter) was the only "interesting" parameter, i.e., bounding the spectral index (or outer gap) by the $\chi^2_{min} + 1$ points. We derived the uncertainties to the spectral indices for the broken power-law fits as was done in Ulmer et al. (1994). We assigned an uncertainty of 10% in all cases for the normalization to reflect an absolute detector calibration uncertainty of this amount. The spectra and the relevant fits are shown in Figures 4–6, and the best-fit values are given in Tables 4 (broken power-law fit) and 5 (power-law and outer gap fits). A brief summary of these results is that P1 is best fitted by an outer gap model; a broken power-law best fits the bridge and P2 regions; the bridge region has the steepest spectrum at energies above the break (spectral index = 2.5), and the bridge also has the highest best-fit break energy of 0.45 MeV; and P2 has a steeper spectrum above the break energy than P1 (spectral index 2.25 vs. 2.09).

We also present results in Table 4 of combining the *CGRO* data with *OSO 8* data. The *OSO 8* (Pravdo & Serlemitsos 1981)

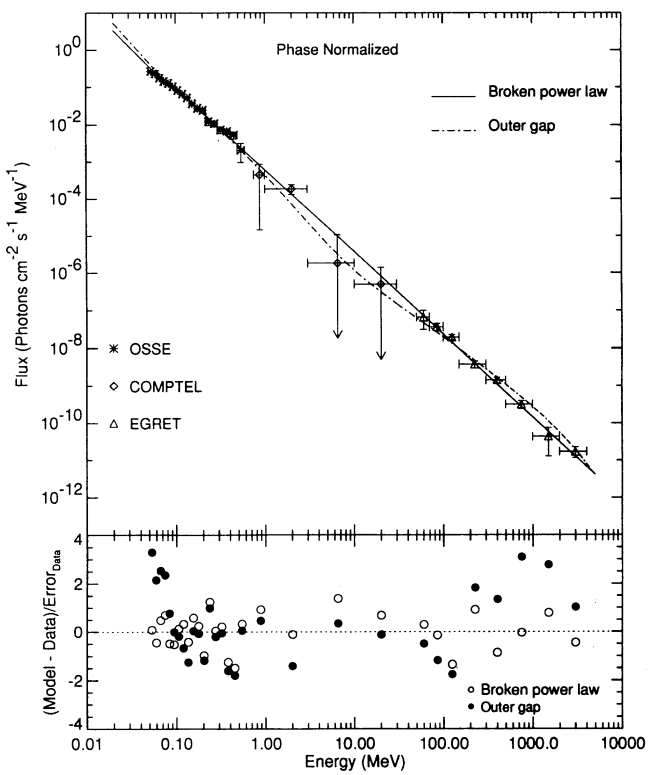

FIG. 3.—*Top*: the phase-averaged total Crab spectrum from OSSE, COMPTEL, and EGRET; the solid line is the best-fit broken power-law model, and the dashed line is the best-fit outer gap model. *Bottom*: the difference between best fit and the data in units of the 1 σ uncertainties in the data.

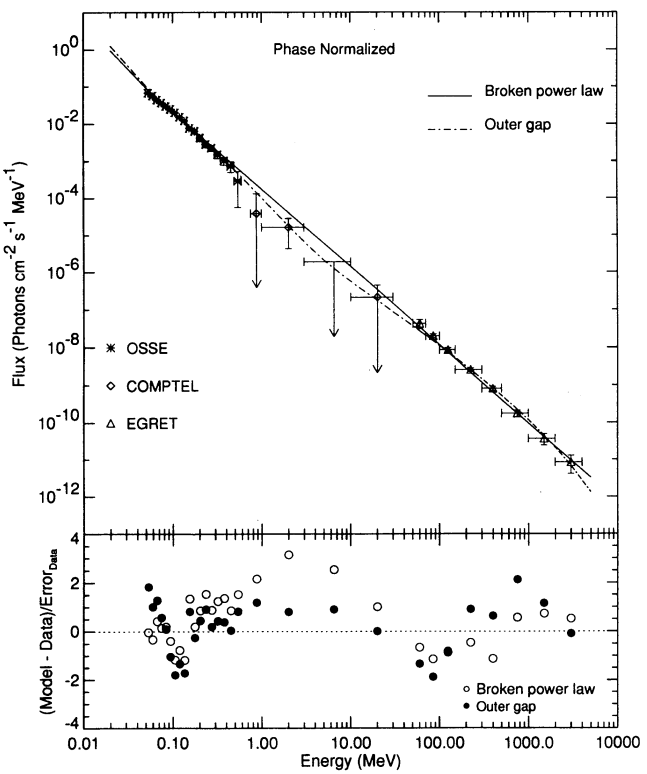

FIG. 4.—*Top*: the P1 region spectrum from OSSE, COMPTEL, and EGRET; the solid line is the best-fit broken power-law model, and the dashed line is the best-fit outer gap model. *Bottom*: same as Fig. 3.

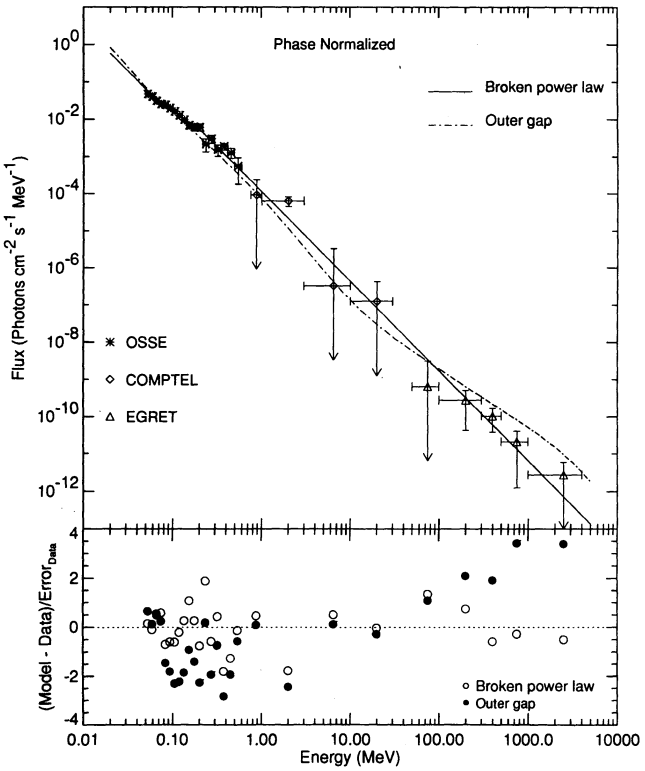

FIG. 5.—*Top*: the bridge region spectrum from OSSE, COMPTEL, and EGRET; the solid line is the best-fit broken power-law model, and the dashed line is the best-fit outer gap model. *Bottom*: same as Fig. 3.

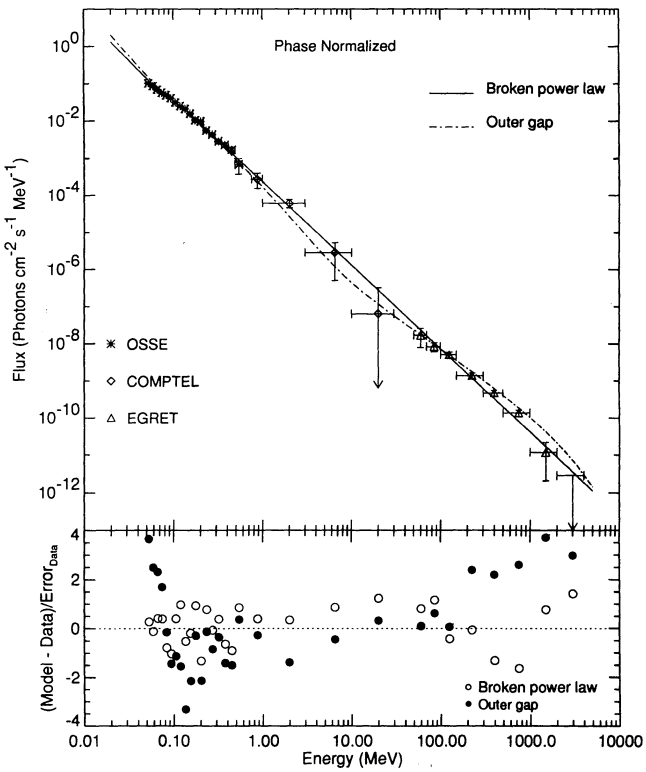

FIG. 6.—*Top*: the P2 region spectrum from OSSE, COMPTEL, and EGRET; the solid line is the best-fit broken power-law model, and the dashed line is the best-fit outer gap model. *Bottom*: same as Fig. 3.

observations are not contemporaneous with those of *CGRO*; assuming that the spectral change and intensity for the total pulse has been negligible, these data can provide a consistency check for the idea that the spectrum flattens as the energy decreases from ~150 keV to 3 keV. This comparison is examined in the next section.

4. DISCUSSION

The combined data from the OSSE, COMPTEL, and EGRET instruments allow us to investigate spectral shapes and light curves over an extended range of gamma-ray energies with high statistical significance. Below we discuss three points

TABLE 4

SUMMARY OF BROKEN POWER-LAW[a] FITS

Region	A	E_B	α_1	α_2	χ^2_{min}	DOF
Total	0.064	0.12 ± 0.03	$1.71^{+0.15}_{-0.19}$	2.21 ± 0.02	16	26
Peak 1	0.026	0.10 ± 0.02	$1.77^{+0.18}_{-0.25}$	2.09 ± 0.01	45	26
Bridge	0.0012	$0.45^{+0.85}_{-0.15}$	1.75 ± 0.12	$2.53^{+0.10}_{-0.23}$	16	23
Peak 2	0.02	$0.13^{+0.02}_{-0.01}$	1.71 ± 0.09	2.25 ± 0.02	21	26
Total + OSO[b].....	0.052	$0.13^{+0.06}_{-0.03}$	$1.85^{+0.03}_{-0.04}$	$2.20^{+0.02}_{-0.01}$	25	37

[a] $F(x) = A(E/E_B)^{-\alpha_1}$, $E \le E_B$; $= E(E/E_B)^{-\alpha_2}$, $E > E_B$, photons cm^{-2} s^{-1} MeV^{-1}.
[b] Best fit with *OSO 8* (Pravdo & Serlemitsos 1981).

TABLE 5

SUMMARY OF POWER-LAW[a] AND OUTER GAP[b] FITS[c]

Region	A	α	E_0	χ_{min}[d]	Gap	Gap N	χ_{min}[d]
Total	0.005	−2.16	0.38	59	0.37	1.07	68
Peak 1.....	0.001	-2.17 ± 0.01	0.38	44	0.450 ± 0.003	0.21	31
Bridge	0.002	−2.24	0.27	60	0.32	0.38	66
Peak 2.....	0.002	−2.18	0.37	128	0.35	0.53	92

[a] $f(x) = A(E/E_0)^a$ photons cm^{-2} s^{-1} MeV^{-1}.
[b] Outer gap model of Ho 1993, modified by allowing the normalization ("gap N" in the table) to vary along with the outer gap parameter ("gap" in the table).
[c] We give uncertainties only for the one model for which there were acceptable χ^2 values, e.g., P1.
[d] dof = 28 for all except the bridge where dof = 25.

in turn: an interpretation of the pulse shape/phase separation (§ 4.1), an interpretation of the spectra (§ 4.2), and a combined interpretation of the spectra and the pulse shape (§ 4.3).

4.1. *Light Curves*

4.1.1. *Peak Separations and Shapes*

Previous studies have suggested that the phase separation shifts with energy by ~ 0.02 from the infrared/UV range (cf. Ransom et al. 1994; Percival et al. 1993; Cordes 1993) to the X-ray range. However, as we have shown in the previous section, there is no statistically significant evidence for any energy dependence in the separation of the peaks in the X-ray–to–gamma-ray energy range (see also Masnou et al. 1994, who come to similar conclusions regarding the separations for the peaks).

We cannot exclude a variation in the peak separation with energy in the X-ray–to–gamma-ray range on the order of 0.01, however. But ambiguities in the peak separation arise (at least in part) because of the method used. For example, choosing the maximum intensity separation value for the X-ray (0.5–3.5 keV) data (Harnden & Seward 1984) produced a value of 0.402 ± 0.002, whereas using Gaussians fitted to the peaks of the OSSE data yielded a value of 0.390 ± 0.002 (Ulmer et al. 1994). While this seems to imply a decrease in phase separation with energy, using the maximum intensity values in the OSSE light curve gives a value of 0.404 ± 0.011. Using more EGRET data with the light curve divided into finer time bins than used here, Ramanamurthy (1994) found (with an unspecified method) a peak separation value of 0.393 ± 0.003, whereas we report here a value of 0.404 ± 0.011. Masnou et al. (1994) found the average value over the 0.15–3.7 MeV energy range to be 0.400 ± 0.005. They used a method different from those we considered, namely a kernel density estimator. Although there *may* be some energy dependence to the peak separation in the X-ray (Harnden & Seward 1984) through the EGRET energy range, the effect is small, and the average peak separation is very close to the radio value of 0.40402 ± 0.0001 (A. G. Lyne 1994, private communication). As an aside we note that Masnou et al. reported a small offset (~ 500 μs) between P1 in the radio and gamma rays, which is too small for us to address with our data.

Of the six known gamma-ray pulsars (see Ulmer et al. 1994 or Thompson 1994 for summaries), only the Crab pulsar has a pulse shape which is approximately the same across the infrared–to–gamma-ray spectrum. It also has approximately the same peak separation across the entire electromagnetic spectrum (over which it has been detected). Any model of gamma-ray pulsars must, therefore, be able to accommodate not only the wide-band similarity of the Crab pulsar but also the disparity of pulse shapes seen in the other pulsars, unless it can be argued that the Crab pulsar is physically different from the other five.

Although the general pulse shapes for the Crab pulsar from the infrared to the EGRET energy range are basically similar in that they have two well-defined peaks and a bridge region, two discrepancies appear: (1) the phase separation of the peaks differs slightly in the IR/visible/UV from that seen in the radio and at high energies, and (2) the P2 (interpulse) is the dominant pulse only in the low-energy gamma-ray range. These differences, and the fact that they appear in disparate parts of the spectrum, suggest that the pulsed emission is not a simple, homogeneous process extending over nearly 15 orders of magnitude in photon energy. It is also interesting to note the similarity between the peak shapes in the optical (Percival et al. 1993) and soft X-ray (Harnden & Seward 1984) energy range.

The variation of phase separation with energy (infrared/optical/UV vs. the gamma rays and radio), although highly significant in statistical terms, is small relative to the total phase. In the radio there are some pulsars (Thorsett 1991; Phillips & Wolszczan 1992, and references therein) which show a definite energy dependence of the phase separation, with the peaks coming closer together at higher frequencies/energies. At the highest radio frequencies, however, the separation becomes constant. The changes in phase with frequency which Thorsett discussed were relatively large (~ 0.3) compared to the small differences seen in the Crab pulsar (~ 0.02). It is not clear, therefore, how to relate the Crab pulsar data to these other double-peaked radio pulsars.

In order for relativistic beaming by high-energy electrons (and positrons) to produce pulses which are closely aligned across a large energy range, it is necessary to assume that all photons are produced in approximately the same location and are produced by electrons accelerated in the same direction (e.g., Ruderman et al. 1993). Furthermore, in order for the 50 keV–10 GeV range peaks to have approximately the same widths (within $\sim 25\%$), the energy of the electrons which produce the radiation over this wide range of energies must be approximately the same. One alternative is to assume that the neutron star magnetic field confines the path of the radiated photon flux into beams.

Although the radio emission represents only a small fraction of the total energy seen at high frequencies, the emission process must be co-aligned with the process which produces the high-energy flux, unless the phase agreement between the radio and gamma rays is considered fortuitous. In addition, the similarity of the radio and gamma-ray pulse separations indicates that the beams share other spatial characteristics. Even if it is assumed that the precursor radio pulse is produced in a different region of the neutron star magnetosphere (e.g., Romani & Yadigaroglu 1995), the main radio pulse and interpulse must somehow be associated with the high-energy emission. The physical processes, however, are unlikely to be the same. The radio emission is generally considered to originate from coherent processes, while the high-energy emission is more likely incoherent. As noted by Percival et al. (1993), both single polar cap (conical emission) and double (two separate) polar cap models can provide acceptable explanations for the pulse shape and its variation with energy in the IR to UV range. By themselves, the pulse shape and separation do not distinguish between models of particle acceleration near the polar caps or in the outer magnetosphere.

Another hypothesis is that the pulsar beams are produced by relativistic bulk motion of the emitting regions relative to Earth. Both Zheleznyakov (1971) and Smith (1970) proposed such a model (isotropic emission in the emission region rest frame) for the pulsar radio emission. We suggest that this isotropic/bulk motion model applies to the higher energy radiation as well. The concept of relativistic bulk motion that we envision is one in which the emitting regions are confined by the neutron star magnetic field at distances close to the light cylinder. It is the rotation of the neutron star, then, rather than motion along the magnetic field lines, that gives rise to the relativistic bulk motion. Within this context, the regions which emit at different wavelengths (radio through gamma-ray) can have different locations relative to the neutron surface. For

example, having a different location is the reason that the maximum intensity points of the infrared, optical, and UV fluxes are offset from the other wavelength bands in P2 . In such a scenario it is not surprising that the gamma-ray spectrum of P1 differs markedly from that of P2, as we discuss in § 4.2 below. A possible difficulty with this bulk motion hypothesis is that the radio and gamma-ray light curves, especially, are so different. The radio peaks are very narrow compared to the gamma-ray peaks, and the radio light curve has no bridge (cf. Lyne & Graham-Smith 1990; Cordes 1993). Perhaps the initial isotropic radio flux is produced in a smaller region than the gamma-ray flux, but the centers of the two emission regions nearly coincide. The near coincidence of the centers explains why the peak separations in the radio and gamma rays are nearly the same.

4.2. *Spectra*

4.2.1. *The Total Pulsed Spectrum*

Ulmer et al. (1994) suggested that the total Crab pulsar spectrum probably changes slope somewhere between ~30 and 200 keV, but the OSSE data were consistent with a single power-law fit to the Crab pulsar spectra. The COMPTEL and EGRET data are needed to significantly constrain the OSSE spectrum to demand a change in slope. Furthermore, if the *OSO 8* data (or other low-energy data; see Ulmer et al., Lyne & Graham-Smith 1990, and references therein) are included, then a change in slope is required regardless of whether OSSE, *HEAO 3* (Mahoney, Ling, & Jacobson 1984), or *GRIS* (Bartlett et al. 1994) data are used. The OSSE, *HEAO 3*, *GRIS*, and *OSO 8* data are compared with each other in Figure 7. Although the *CGRO* flux best fit alone does extrapolate to systematically lower values than the *OSO 8* data, the *CGRO* broken power-law best fit does not differ in a statistically significant manner from that derived with the *OSO 8* data included.

Furthermore, it can be seen that there are ~30% differences among the OSSE, *GRIS*, and *HEAO 3* results. We quote a 10% overall absolute uncertainty for the *CGRO* data, and uncertainties at least this large are probably extant in data sets such as the *GRIS* and *HEAO 3* data sets. Therefore, we consider the spectra shown in Figure 7 to be in general agreement.

Finally, in Figure 7 it can be seen that there is an apparent curvature or change in slope in the OSSE data relative to the *GRIS* data. As noted above, however, the OSSE data alone are statistically consistent with a single power-law spectrum (cf. Ulmer et al. 1994), so that this apparent curvature is simply an indication of a difference in the best-fit power-law slopes.

It is possible to interpret the break in a power-law spectrum as being related to particle lifetimes in a magnetic field (cf. Knight 1982). But the variations in spectral shape across the pulse (as discussed below) suggest that it is no longer relevant to produce a detailed model for the total Crab pulsar spectral shape.

4.2.2. *Interpretation of the Phase-resolved Spectra*

Regardless of detailed model fitting or absolute calibration uncertainties (e.g., the differences among *GRIS*, OSSE, and *HEAO 3*), the following can be deduced: (*a*) the relative intensities of the various regions (P1, bridge, and P2; see Fig. 1) change with energy so that the spectrum must change; (*b*) P1 (Fig. 4) has a high 100 MeV flux compared to the extrapolation of the ~150 keV to 10 MeV spectra (above any break that may exist near 100 keV in the average pulse spectrum), which leads to P1 being best fitted by an outer gap model, although a broken power-law or a single power-law model cannot be strictly excluded on statistical grounds (we refer to this in the summary section as an "excess flux near 100 MeV"); and (*c*) the P2 (Fig. 6) and the bridge (Fig. 5) are both best fitted by a broken power law.

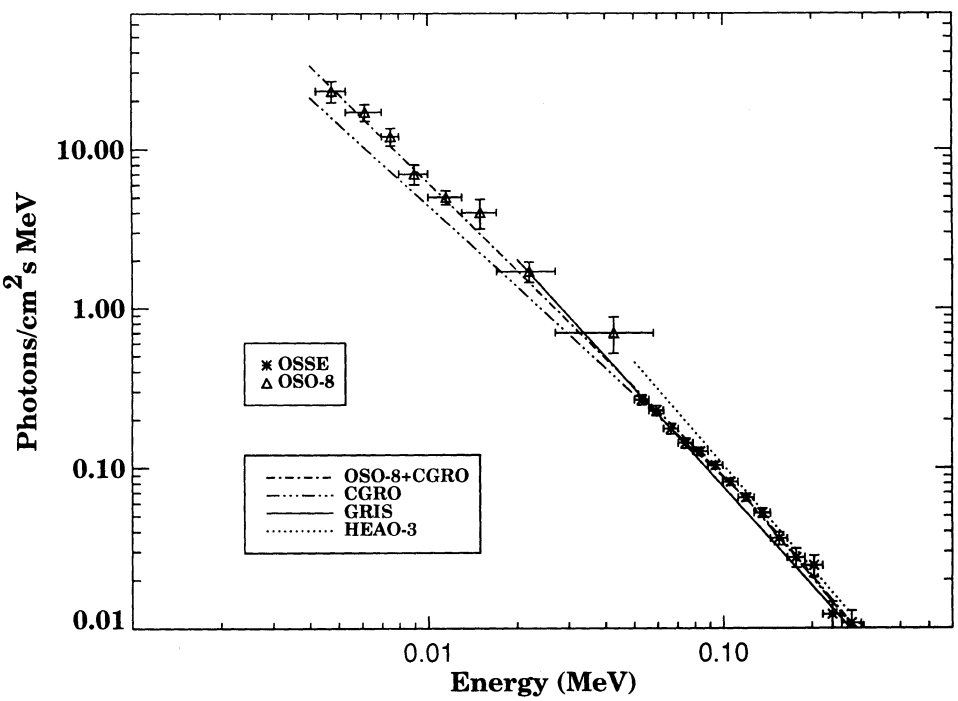

FIG. 7.—A comparison of spectra from various experiments; see text for references. "CGRO" refers to the best fit to the OSSE, COMPTEL, and EGRET spectra combined.

Before continuing, we note that Nolan et al. (1993) produced phase-resolved spectra for the EGRET data alone. The number of detected photons was so small that the inference of a flatter bridge region spectrum was not statistically significant. It is this very statistical uncertainty that allowed us to derive a result that is apparently in conflict with the Nolan et al. result. There are, therefore, at least two possibilities: (*a*) the gamma-ray bridge spectrum is indeed steeper, as inferred from our best fits here, or (*b*) the bridge spectrum flattens in the range above about 100 MeV. Such a change in spectral shape can be understood within the context of an inverse-Compton model discussed below. For simplicity, however, we will explicitly discuss only possibility (*a*).

Although interpretation of these data in the context of detailed theoretical models of pulsar gamma-ray spectra is desirable, such modeling of the data over the *CGRO* energy range is beyond the reach of currently published theories (see, for example, Much et al. 1994, Percival et al. 1993, Ho 1993, and references therein). We therefore confine ourselves to a phenomenological discussion below.

The best fit to the P1 spectrum (from among the models considered here[1]) is provided by an outer gap model. A key feature of the outer gap model (Ho 1993; Cheng et al. 1986a, b) is that there is a photon field that is extant to be boosted to higher energies by relativistic electrons/positrons via the inverse-Compton process.[2] That the bridge and P2 spectra are different from that of P1 is consistent with the infrared, optical, and UV light curves also being different from the $\sim$50 keV to 10 MeV gamma-ray light curves (see, for example, our Fig. 1, and Percival et al. 1993; Cordes 1993; Ransom et al. 1994). In the next section we combine this hypothesis of coincident relativistic electrons and infrared, optical, and UV photons with a scenario for producing the light curves.

4.2.3. *Interpretation of the Light Curves and Spectra Combined*

We now offer the following as simply *one* interpretation. We are *not* suggesting that this is necessarily the correct/unique interpretation of the data. The interpretation is as follows: The fluxes in all wavelength bands are produced isotropically in their rest frames. The beams observed at Earth are the result of relativistic bulk motion relative to Earth. The variations in light curves with wavelength indicate that these isotropically emitting regions are not exactly coincident with each other. The gamma-ray spectrum above $\sim$100 MeV is in large part produced by the inverse-Compton process where the lower energy (infrared to UV, say) photons coexist with the requisite energy ($\sim$1 to 10 GeV, say) electrons. Then the lack of low-energy photons in the bridge and P2 regions (Percival et al. 1993; Cordes 1993; Ransom et al. 1994) gives rise to the relative (to P1) deficit of $\sim$100 MeV photons in the bridge and P2 regions. Further, relativistic bulk motion requires that the emitting regions exist close to the magnetic field light cylinder rather than close to the neutron star surface. Then the scenario we introduced here implies that the regions responsible for P1, the bridge, and P2 are all physically separated. In this picture P1 comes from a much different region than P2, which is consistent with the observation that P1 produces many more giant radio pulses than P2 (cf. Lundgren et al. 1995).

[1] Published polar cap spectral models have not been extended down to 50 keV (cf. Harding & Daugherty 1993).

[2] The Crab-type outer gap involves the production of primary photons via curvature radiation; however, the model invokes Compton scattering from secondary e^+e^- pairs to produce the flux above about 10 MeV.

5. SUMMARY AND CONCLUSIONS

We have presented simultaneous observations of the Crab pulsar covering the energy range from 50 keV to 10 GeV. We have found that the phase of P1 is consistent with being coincident with the radio phase to within the 300 μs (3 σ) accuracy of the radio measurement of the absolute phase. We have also found the peak separations to be constant to within 0.02 with an average value of 0.4. This is consistent with the value found in the radio and about 0.015 lower than that observed in the optical and UV by Percival et al. (1993). A limit to any energy-dependent effects in the hard X-ray/gamma-ray peak separation is a factor of 10 or more smaller than those seen in several double-peaked radio pulsars (cf. Thorsett 1991; Phillips & Wolszczan 1992).

We also measured the width of the peaks and found that the widths of the $\sim$100 keV light curve peaks were the same to within $\sim$25% as those at $\sim$100 MeV. All of these properties lead us to suggest a scenario in which the radiation is isotropic in the rest frame of the neutron star. The shapes of the gamma-ray peaks and their separation are the result of bulk motion relativistic beaming. The radio beams may be produced in much the same manner as suggested by Smith (1970) and Zheleznyakov (1971), but the radio and gamma-ray beams are disparate in shape. The difference in shape between the radio and gamma-ray light curves is yet to be explained, but it may be due to the radio-emitting region being much smaller than the gamma-ray–emitting region.

The phase-resolved spectroscopy showed that the spectra of the peaks and the bridge all differ considerably from each other. The P1 spectrum has an excess flux near 100 MeV compared to the average. The bridge and P2 regions have deficits of flux near 100 MeV, with the bridge region having the larger deficit. This can be explained in the context of a model in which the gamma-ray spectrum is at least in part the result of inverse-Compton–scattering of infrared, optical, and UV photons, with the number of target photons available being proportional to the observed intensity of the light curve in the infrared, optical, and UV. Although many details of the pulsar emission process are missing in this picture, we hope it will provide the impetus for further theoretical and observational investigations.

We thank the radio astronomers (Z. Arzoumanian, D. Nice, J. Taylor, S. Lundgren, and J. Cordes) for providing the data for the ephemerides. We thank C. Ho for providing the code for this outer gap model. This work was supported in part by NASA grant DPR S-10987C.

REFERENCES

Arons, J. 1984, Adv. Space Res. 3(10–12), 287
Arzoumanian, Z., Nice, D., & Taylor, J. H. 1992, GRO/Radio Timing Database, Princeton Univ.
Bartlett, L. M., Barthelmy, S. D., Gehrels, N., Teegarden, B. J., Tueller, J., Leventhal, M., & MacCallum, C. J. 1994, in The Second Compton Symposium, ed. C. E. Fichtel, N. Gehrels, & J. P. Norris (New York: AIP), 67
Cheng, K. S., Ho, C., & Ruderman, M. 1986a, ApJ, 300, 500
———. 1986b, ApJ, 300, 522
Cordes, J. M. 1993, in Isolated Pulsars, ed. K. A. Van Riper, R. Epstein, & C. Ho (Cambridge: Cambridge Univ. Press), 182
Daugherty, J. K., & Harding, A. K. 1982, ApJ, 252, 337
Dermer, C. D., & Sturner, S. J. 1994, ApJ, 420, L75

Harding, A. K., & Daugherty, J. K. 1993, in Isolated Pulsars, ed. K. A. Van Riper, R. Epstein, & C. Ho (Cambridge: Cambridge Univ. Press), 279
Harnden, F. R., Jr., & Seward, F. D. 1984, ApJ, 283, 279
Hasinger, G. 1984, Ph.D. thesis, Ludwigs-Maximilians-Univ.
Hasinger, G., Pietsch, W., Reppin, C., Trümper, J., Voges, W., Kendziorra, E., & Staubert, R. 1984, Adv. Space Res., 3(10–12), 63
Ho, C. 1993, in Isolated Pulsars, ed. K. A. Van Riper, R. Epstein, & C. Ho (Cambridge: Cambridge Univ. Press), 271
Johnson, W. N., et al. 1993, ApJS, 86, 693
Knight, F. K. 1982, ApJ, 260, 538
Lundgren, S. C., et al. 1995, in preparation
Lyne, A. G., & Graham-Smith, F. 1990, Pulsar Astronomy (Cambridge: Cambridge Univ. Press)
Mahoney, W. A., Ling, J. C., & Jacobsen, A. S. 1984, ApJ, 278, 784
Masnou, J. L., et al. 1994, A&A, 209, 503
Much, R., et al. 1994, A&A, in press
Nolan, P. L., et al. 1993, ApJ, 409, 697
Percival, J. W., et al. 1993, ApJ, 407, 276
Phillips, J. A., & Wolszczan, A. 1992, ApJ, 385, 273
Pravdo, S. H., & Serlemitsos, P. J. 1981, ApJ, 246, 484
Ramanamurthy, P. V. 1994, A&A, 284, L13
Ransom, S. M., Fazio, G. G., Eikenberry, S. S., Middleditch, J., Kristian, J., Hays, K., & Pennypacker, C. R. 1994, ApJ, 431, L43
Romani, R. W., & Yadigaroglu, I.-A. 1995, ApJ, 438, 314
Ruderman, M., Chen, K., Cheng, K. S., & Halpern, J. P. 1993, in Compton Gamma-Ray Observatory, ed. M. Friedlander, N. Gehrels, & D. J. Macomb (New York: AIP), 259
Schönfelder, V., et al. 1993, ApJS, 86, 657
Smith, F. G. 1970, MNRAS, 149, 1
Sturner, S. J., & Dermer, C. D. 1994, ApJ, 420, L79
Thompson, D. J. 1994, in The Second Compton Symposium, ed. C. E. Fichtel, N. Gehrels, & J. P. Norris (New York: AIP), 57
Thompson, D. J., et al. 1993, ApJS, 86, 629
Thorsett, S. E. 1991, ApJ, 377, 263
Ulmer, M. P. 1994, ApJS, 90, 789
Ulmer, M. P., et al. 1993, ApJ, 417, 738
Ulmer, M. P., et al. 1994, ApJ, 432, 228
Zheleznyakov, V. V. 1971, Ap&SS, 13, 87